Interpretation of Multigated Fourier Functional Images

Richard E. Wendt III, Paul H. Murphy, John W. Clark, Jr., and John A. Burdine

Rice University, Baylor College of Medicine, St. Luke's Episcopal and Texas Children's Hospitals and the Texas Heart Institute, Houston, Texas

First-harmonic Fourier analysis is currently used to aid in the interpretation of multigated cardiac studies. Its intrinsic inaccuracies are not generally appreciated. This study investigates the characteristics and magnitudes of the errors of this technique. The study analyzes computer-generated phantoms that isolate the various motions of the ventricles (contraction, translation, and rotation) with the first-harmonic approach. The first-harmonic output is compared with a more accurate fitting scheme using multiple terms of the Fourier expansion. Significant artifacts of the inaccuracy of the first harmonic appear in the phantom studies and are observed in patient examples. We conclude that caution is needed in interpreting first-harmonic phase and amplitude images, and particularly in associating them with parameters like the onset of contraction and the stroke volume.

J Nucl Med 23: 715–724, 1982

"Phase analysis" of multigated cardiac blood-pool studies has grown in popularity in the last few years (*1*,*2*,*16*). The essence of temporal Fourier analysis of multigated studies is that each pixel describes a periodic time series. Thus the behavior during the R-R interval of each element of the field of view of the camera is independently characterized. The construction of Fourier functional images allows the visualization of the spatial distribution of this temporal behavior. Inspection of Fig. 1a reveals the rough approximation of the data points by the first Fourier harmonic. While it is customary to associate the phase ϕ_1 of the first harmonic with the time at which ejection starts, there can be a significant difference between the two times for time-activity curves similar to the one in Fig. 1. The relationship of the magnitude of the first harmonic, SV′, to the stroke volume of the data points is not exact either. Bacharach et al. (*3*), have presented a study that demonstrates this problem for a range of simulated global volume curves.

The results of the present work arose from an effort to understand better what information is contained in the first-harmonic-phase functional images. In such images taken from normal 45° LAO studies, the point in the R-R interval indicated by the phase is generally earlier near the base of the left ventricle than at its apex. This agrees with recent work on the sequence of contraction of the left ventricle (*8*). Nevertheless, the absolute times indicated by the first-harmonic phase do not correspond to the onset of contraction, and the relative timing does not agree with published data.

To isolate and study particular aspects of the phase images, we have developed a set of computer-generated phantoms. To address the problem posed by the poor fit of the first harmonic to time-activity curves, additional harmonics are used in a multiharmonic approximation. The latter has more degrees of freedom, so many distinct functional images can be constructed.

METHODS

The discrete Fourier transform of a pixel's time-activity curve is defined to be (*14*)

Received Dec. 28, 1981; revision accepted Apr. 8, 1982.

For reprints contact: Paul H. Murphy, PhD, Nuclear Medicine Service, St. Luke's Episcopal and Texas Children's Hospitals, 6720 Bertner, Houston, TX 77030.

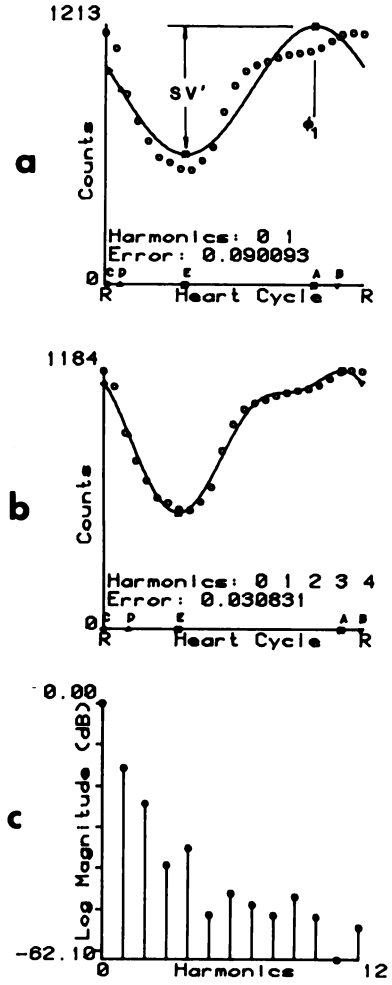

FIG. 1. (a) First-harmonic fit to a simulated left-ventricular volume curve. Data points are indicated by circles and the fit by the solid line. Error is the sum of squared differences of the fit at the data points and the data points themselves, normalized by the sum of the squares of the data points. Thus the most naive fit, a horizontal line with value zero, will have an error value of 1.0. (b) Improvement in fit due to including second, third, and fourth harmonics in the approximation. Values of higher harmonics have been weighted in order to produce an approximation without ringing. Points indicated by letters directly above time axis are parameters of the approximation. (A) is time at which maximum occurred. (B) is start of ejection as determined by slope of curve. (C) is start of ejection as indicated by a decrease in counts of 20% of the stroke. (D) is time at which maximum negative slope occurred. (E) is time at which the minimum occurred. (c) Magnitude spectrum, indicating significance of first four harmonics. This is a typical shape for the magnitude spectrum of left-ventricular global volume curve. It is "low-pass," with fourth harmonic as large as or larger than the third, and fifth and higher harmonics much lower in magnitude.

$$X(k) = \sum_{n=0}^{N-1} x(n)e^{-j2\pi kn/N} = \sum_{n=0}^{N-1} x(n)\cos(2\pi kn/N) - j\sum_{n=0}^{N-1} x(n)\sin(2\pi kn/N), \quad (1)$$

where N is the number of frames in the study, n is the frame number within the study, x(n) is the value of a pixel in frame n, k is the harmonic number, X(k) is the complex-valued k*th* harmonic, and j is the usual imaginary identity, equal to $\sqrt{-1}$. The inverse transformation is

$$x(t) = \frac{1}{N}\sum_{k=0}^{N-1} X(k)e^{j2\pi kt/N} = \sum_{k=0}^{N-1} a_k \cos(2\pi kt/N + \phi_k), \quad (2)$$

where $a_k = 1/N\{ReX(k)]^2 + [ImX(k)]^2\}^{1/2}$, the scaled magnitude of the k*th* harmonic, ϕ_k = arctan [ImX(k)/ReX(k)] is the phase angle of the k*th* harmonic, and $0 \leq t < 1$ is time, normalized to the R-R interval.

Referring again to the forward transformation in Eq. (1): since the pixel values x(n) are real-valued, the real-valued part of the k*th* harmonic, ReX(k), has even symmetry and the imaginary-valued part of the k*th* harmonic, ImX(k), has odd symmetry. Since the squaring operation used to get the k*th* magnitude is an even function, it follows that the magnitude a_k has even symmetry, which (for an even number N of frames in the study) implies that $a_k = a_{N-k}$ and that a_0 and $a_{N/2}$ are special cases. Likewise, since the arctangent function that gives the k*th* phase is an odd function, the k*th* phase ϕ_k has odd symmetry, $\phi_k = -\phi_{N-k}$ (for $[k \neq 0$ or $N/2]$). The inverse transformation of Eq. (2) can be approximated for pixel time-activity curves by

$$\hat{x}(t) = w_0a_0 + 2\sum_{k=1}^{m} w_ka_k \cos(2\pi kt/N + \phi_k), \quad (3)$$

where the w_k are weighting factors that reduce ringing artifacts in the approximation, and the (N/2)*th* term is ignored.

The first harmonic (FH) approximation, then, is

$$\hat{x}_{FH}(t) = a_0 + 2a_1 \cos(2\pi t/N + \phi_1), \quad (4)$$

and is shown for a simulated global left-ventricular volume curve in Fig. 1a.

Figure 1c is a magnitude spectrum of the volume curve. It compares the logarithm of the magnitude, $\log(a_k)$, to the harmonic number k. The spectrum is "low-pass," meaning that the value of a_k decreases as k increases. For the multiharmonic (MH) approximation,

$$\hat{x}_{MH}(t) = a_0 + 2\sum_{k=1}^{4} w_ka_k \cos(2\pi kt/N + \phi_k), \quad (5)$$

the first four harmonics are used, with weighting factors $w_0 = w_1 = 1.0$, $w_2 = 0.853$, $w_3 = 0.5$, and $w_4 = 0.146$ corresponding to a modified Hanning filter (*4*). The use of additional harmonics to approximate the time-activity curves is discussed in Refs. *9* and *17*, and apparently they were used implicitly by Verba et al. (*16*).

An important consideration in the interpretation of functional images is that the camera, and hence the pixel, is stationary in space during the collection of a multigated study. The physical movement of radioactivity relative to the camera can be divided conceptually into

motion parallel to the plane of the pixel and motion perpendicular to it. In the former case, changes in the density of the pixel with time would be due to a rigid structure of nonuniform thickness that is sliding past the pixel. In the latter case, a stationary structure of uniform but time-varying thickness would be viewed by the pixel. A complete description of a time-activity curve involves both types of motion.

The computer-generated phantom studies were developed to combine these two types of motion in a controlled manner. We emphasize that these phantoms are not intended to simulate the motion of the cardiac blood pools with great fidelity. Rather, by their very simplicity, they isolate and emphasize particular aspects of what is, in fact, a complicated motion. The use of terms like "end-diastolic" is for the purpose of analogy, and not to claim an exact correspondence between the phantoms and actual clinical data.

In essence, all of the phantoms are of simple geometric solids whose volumes change according to the global volume curve shown in Fig. 1. Each frame of a study is composed of pixels whose values are determined by the thickness of the figure projection onto each pixel. The size of the figure is computed from the value of the global volume curve at the time of that frame. The details of the generation of the phantoms are given in the appendix.

The first phantom is of a solid cylinder, viewed from an end, whose thickness is constant throughout the "heart beat" but whose radius changes to reflect a global volume curve like that in Fig. 1. This is shown diagramatically in Fig. 2a. The study frames show a succession of circles of constant intensity throughout the study; they first decrease in diameter until, at "end-systole," they start to increase again.

The other phantoms share a common element, a two-dimensional projection of a sphere whose global volume curve has the same shape as the curve of Fig. 1. Figures 2–8 show representative frames and first-harmonic phase images from each of the phantom studies. In the second phantom (Fig. 2b), two spheres "beat" 180° out of phase, with their edges always just touching, approximating a nonoverlapping atrium and ventricle. In the third, two spheres overlap (Fig. 2c). The global volume curve for the upper sphere is based on the shape of a representative left-atrial volume curve (*5*). The fourth phantom (Fig. 2d) is of a single sphere with a slice removed, as if it were two hemispherical chambers, e.g., the ventricles, with a septum. As the sphere beats, it also rotates through 20° about an axis through its center, parallel to the septum. In the frames of this study one sees the split sphere shrink and expand during the course of the phantom study, and the septal area becomes blurred and then sharp once again as the pixel "sees" projections of the side, rather than the edge, of the septum. The last phantom is of a beating sphere with a septum in which the additional motion is a translation

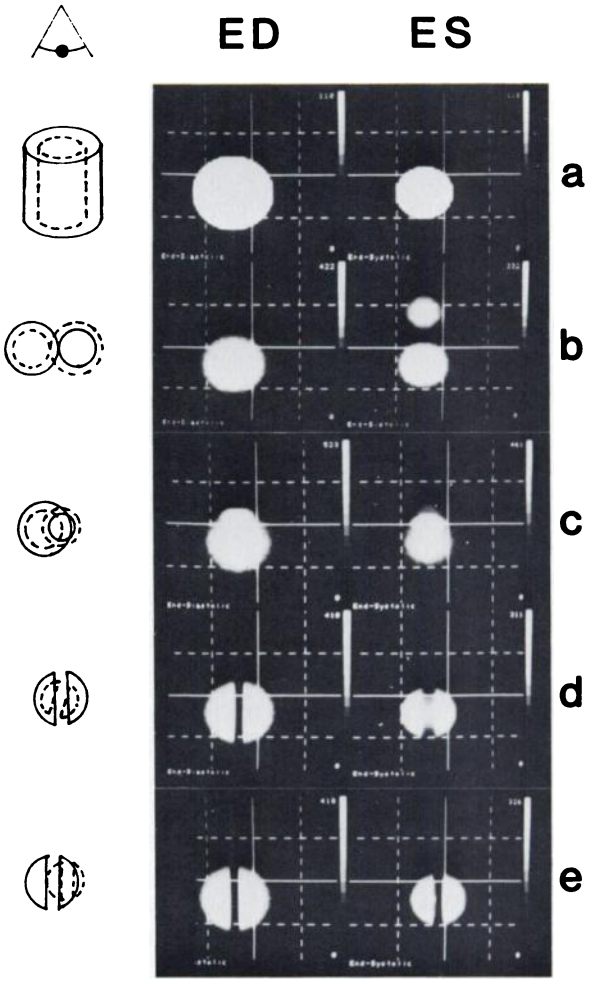

FIG. 2. Phantom studies described by schematics of their motion in first column, their end-diastolic images in second column, and their end-systolic images in third column. In first column, the point of view of scintillation camera is from above. (a) Cylindrical phantom whose thickness remains constant, but whose radius varies. (b) Phantom of two spheres whose edges just touch. Larger sphere has global volume curve of Fig. 1. Smaller sphere has a global volume curve like that of left atrium. (c) Phantom of two overlapping spheres. Again, larger sphere has global volume curve of Fig. 1 and smaller sphere has a global volume curve like that of left atrium. (d) Rotating septal phantom. Sphere has a slice removed. At the R wave, observer is looking edgewise at the septum, but as time progresses toward end-systole, sphere contracts and also turns, so that observer is looking from side of sphere. (e) Shifting sphere. As sphere contracts it also moves to the right.

to and fro, shown in Fig. 2e.

The patient data presented later as illustrative examples were collected in frame mode with a 200-msec tolerance in the R-R interval. Each study has 24 frames in a 64 × 64 matrix. The termination parameter was 12 million counts, resulting in about 200,000 counts per frame using an acquisition zoom factor of approximately 1.5. A 45° LAO projection was used with a medium-resolution collimator after in vivo labeling of Tc-99m red blood cells. These images were smoothed with a standard nine-point smoothing algorithm. The problem of loss of counts in the last frames due to variation in the R-R in-

terval was compensated for by multiplying each pixel of a smoothed, deficient frame by a correction factor. The factor was chosen for each deficient frame so that the corners of the image have the same number of counts as the average of the corners of the frames in the first half of the study.

At this point, the processing is the same for the phantom studies and for smoothed and compensated patient data. The discrete Fourier transform is implemented by a fast Fourier transform (FFT) algorithm (*14*). It is applied to each pixel of the study, and the magnitudes and phases are calculated and stored. On a PDP-11/55 computer, a 24-frame study takes about 6.5 min of computer time, and on a PDP-11/34A up to 25 min. The program is written to run in 32k words of main memory. If less memory were available, the time cited above would increase, since more disk accesses would be required.

The techniques for multiharmonic analysis are mainly iterative in nature. An appropriate function of the approximation, Eq. (3), is solved for its zeros, using Newton's method (*12*). A typical example is the multiharmonic time of maximum. Since the first-harmonic phase indicates the maximum of the first-harmonic approximation, it is interesting to compare it with the maximum of the multiharmonic approximation. To find the time of maximum of the multiharmonic approximation to the pixel time-activity curve, the algorithm finds the zeros of the first derivative of the approximation and then chooses the larger value of the multiharmonic approximation at those points. The iterative routine,

$$t_{m+1} = t_m - f(t_m)/f'(t_m), \qquad (6)$$

where m is the iteration index,

$$f(t) = \frac{d\hat{x}_{MH}(t)}{dt} = \frac{-4\pi}{N} \sum_{k=1}^{4} k w_k a_k \sin\left(\frac{2\pi kt}{N} + \phi_k\right),$$

and

$$f'(t) = \frac{d^2\hat{x}_{MH}(t)}{dt^2} = \frac{8\pi^2}{N^2} \sum_{k=1}^{4} k^2 w_k a_k \cos\left(\frac{2\pi kt}{N} + \phi_k\right),$$

is run until a suitable stopping criterion, based on the resolution of the color table of the video display, is reached. The starting value is determined by a coarse search of the function over the R-R interval. Other temporal multiharmonic parameters are calculated in a similar manner. Amplitude parameters, like maximum excursion or maximum negative rate of exchange, are calculated by evaluating the approximation at particular points in the R-R interval. For example,

$$\text{Maximum excursion} = \hat{x}_{MH}(\text{time}_{\text{maximum}}) - \hat{x}_{MH}(\text{time}_{\text{minimum}}). \qquad (7)$$

Other temporal multiharmonic parameters that have been investigated include the time-of-minimum counts, the time of maximum negative rate of change of counts, and two measures of the onset of contraction. One onset parameter is the time at which 20% of the pixel stroke has occurred, and the other is the time of intersection of the horizontal line through the maximum of the curve and the line tangent to the curve at the point of maximum negative slope. In Fig. 1b these are indicated by the lettered points along the horizontal axis, and identified in the caption. Another amplitude multiharmonic parameter is the magnitude of the maximum negative slope. On the PDP-11/55 the calculation of six multiharmonic functional images takes about 15 min of computer time. This time varies, depending on the particular study, since the algorithm is iterative and it assumes that the Fourier transform data have already been obtained.

RESULTS

The phantom studies display some interesting first-harmonic phase patterns. Figure 3 shows data from the cylindrical phantom (see Fig. 2a). The time indicated by the phase has its earliest value at the end-systolic outline, and becomes later near the end-diastolic border. This is subsequently referred to as the "edge effect" since it is evident in the region through which the edge of the chamber moves during the R-R interval. The spherical phantom in Fig. 4 (see Fig. 2b) shows a similar effect, more clearly visible in the lower sphere. Again, the edge effect is evident, since the time indicated by the phase is later near the end-diastolic edge than near the end-systolic outline. Within the end-systolic outline, however, the time becomes slightly later. Notice the clear demarcation between the two spheres in the phase image. In Fig. 5 (see Fig. 2c) the spheres overlap, producing an anomalous region in the phase image where the overlap occurs. Figure 6 (see Fig. 2d) shows an abrupt change in phase value in the "septal" region of the rotating-sphere phantom. The translating phantom in Fig. 7 (see Fig. 2e) has a wide range of phase values, illustrating the result of a shifting count density. In all of these phantoms, if the phase were to be interpreted as an indication of "systolic contraction," it should be uniform in value, since every portion of the simulated chamber begins to "contract" at the same time.

The patient examples show many of the same features. Figure 8 is representative of our experience with a normal phase pattern for wall-motion studies in the 45° LAO projection. The pattern in the left ventricle is earliest in the basal region and proceeds over the ventricle to the apex. The histogram of the amplitude-masked phase image shows the two-peaked appearance commonly reported for the first-harmonic phase. The peak corresponding to the ventricles is centered substantially before the R wave. In a normal patient, one would expect ventricular contraction to occur shortly after the R wave. The free wall of the left ventricle is slightly later than the

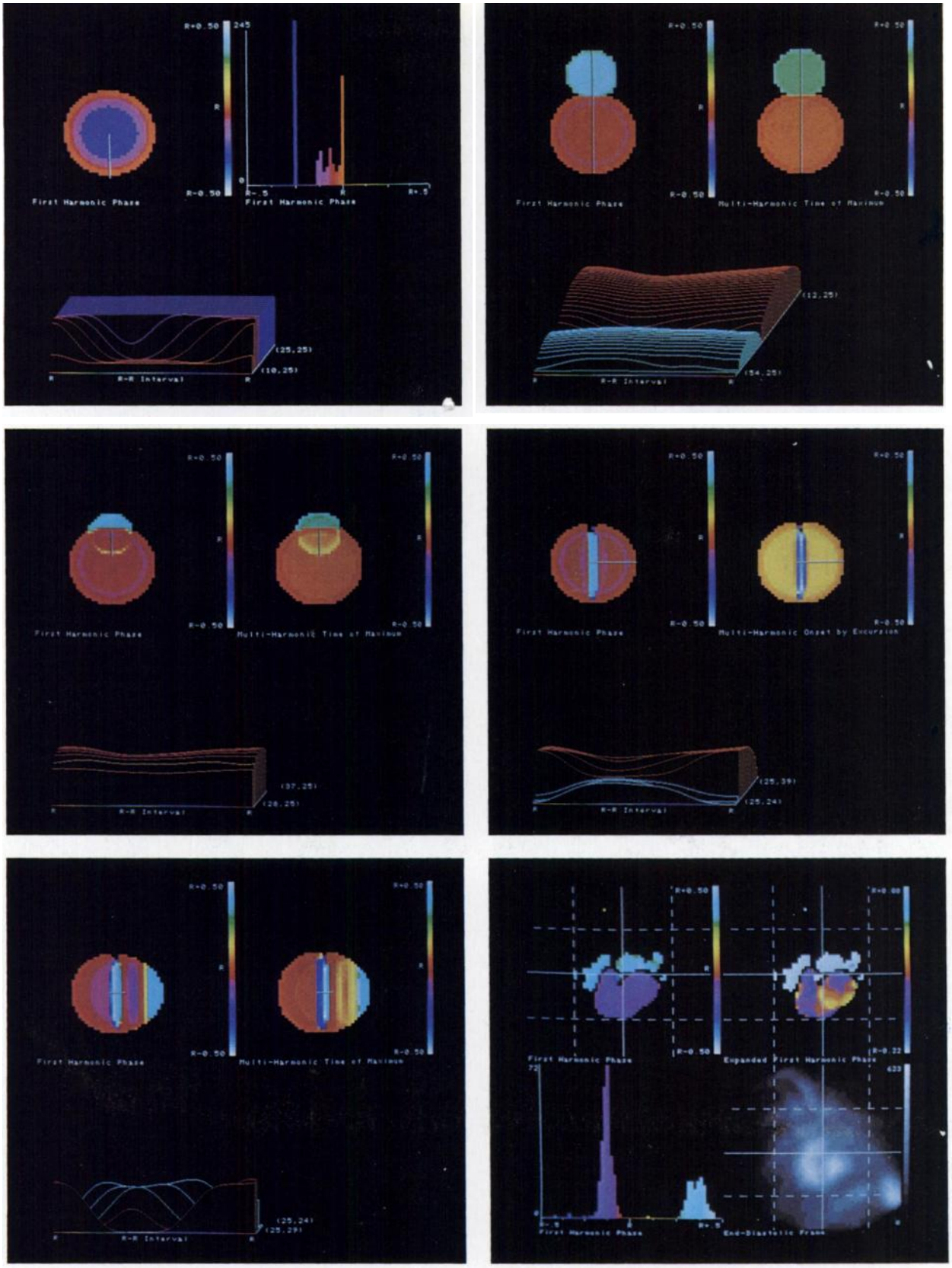

FIG. 3. Upper left-hand (UL) image is first-harmonic phase of cylinder phantom in Fig. 2a. Image is coded in time relative to R-R interval. Time-color relationship is indicated by labels next to color table. R wave is coded as orange. Time increases through green to white. Color table then wraps around to the bottom and time continues through blue until it reaches next R wave. Upper right-hand (UR) panel is histogram of UL, showing number of pixels possessing phase values within each 6° interval. At bottom of figure is a count-rate profile along the contour indicated by white line in UL. This is a stack of pixel time-activity curves for pixels cut by the contour. Time is plotted horizontally, counts vertically. Depth is position along contour. Since lower left-hand corner of an image is point (0,0) and upper left-hand corner is point (63,0), direction along contour can be determined from depth legend. In this case contour is from edge in to center. Each curve is color-coded by value of first harmonic of corresponding pixel.

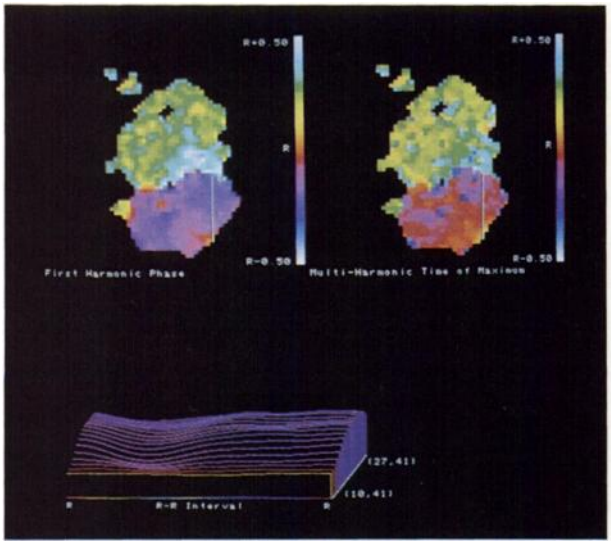

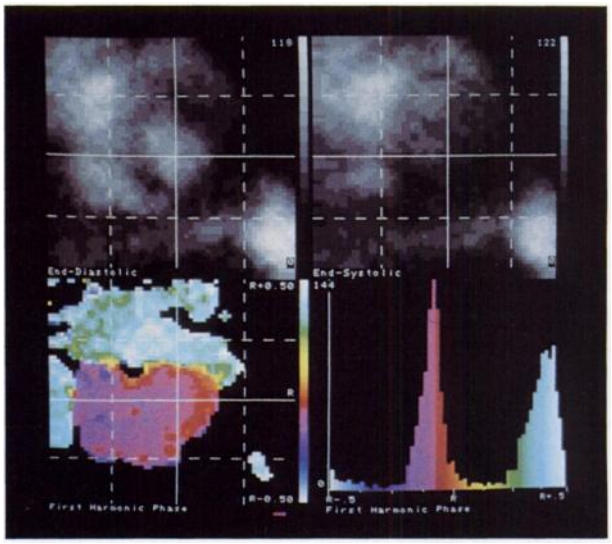

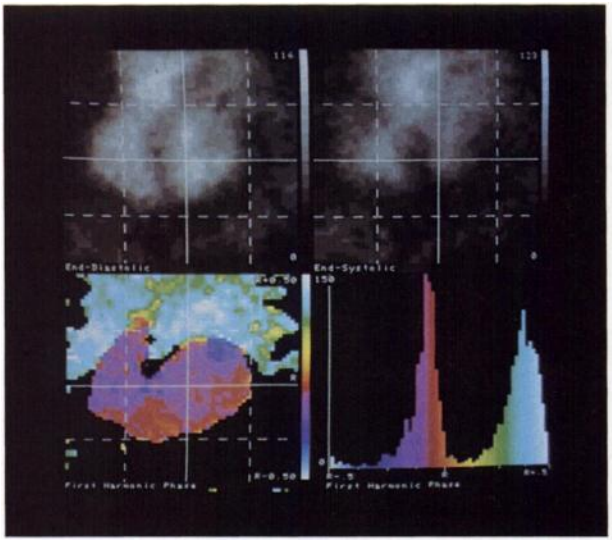

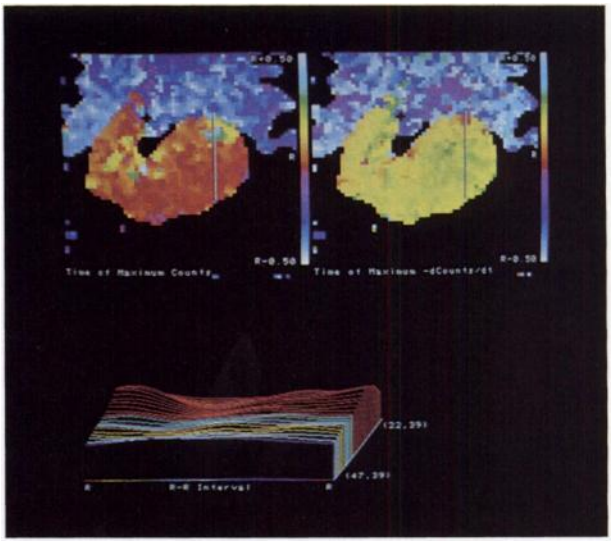

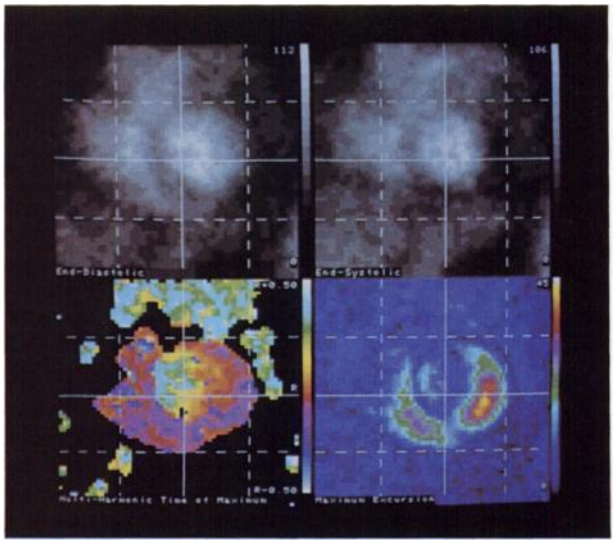

FIG. 4. (upper right, p 719) UL is first-harmonic phase image of the two adjoining spherical phantoms. UR is multiharmonic time-of-maximum functional image. At bottom is count rate profile through centers of both spheres, color-coded by first-harmonic phase values.

FIG. 5. (center left, p 719) Format is as in Fig. 4. Count-rate profile is of region of overlap of the two spherical phantoms. Double peaks of some of the pixel time-activity curves show combined effect of the two chambers.

FIG. 6. (center right, p 719) This is rotating septum phantom. Upper left is first-harmonic phase functional image. UR is multiharmonic image of time of onset of ejection as determined by a magnitude criterion: when change in counts was negative and equal in magnitude to 20% of stroke volume for pixel, ejection was defined to have commenced unequivocally. At bottom is count-rate profile starting at edge of septum in end-diastolic image, and cutting along to the edge. It is color-coded by phase values of pixels. While first harmonic barely distinguishes details of time-activity curves of septum, onset-of-contraction image makes asymmetry of the two outer pixels of the septum quite vivid.

FIG. 7. (bottom left, p 719) Phantom of sphere that translates as it contracts. UL is first-harmonic phase image and UR is multiharmonic time-of-maximum functional image. Effect of shift is to produce a region in the functional images of vividly paradoxical value, since pixels in those regions are at background level near the R wave.

FIG. 8. (bottom right, p 719) Patient study typical of our experience with a normal first-harmonic phase pattern. UL is first-harmonic phase functional image. UR is same first-harmonic phase image, with color table expanded in phase region corresponding to ventricles. Earliness in left-ventricular base and lateness around periphery of left ventricle are demonstrated. These images have been masked by the amplitude image so that background, which has

interior region of the left ventricle. The overall spread in phase from the base to the apex is roughly one tenth of the R-R interval, or 80 msec, in this patient.

Figure 9 is from a patient with a relatively slow heart rate. The first-harmonic phase image is markedly shifted away from the R wave in the ventricles.

The studies shown in Fig. 10 compare the absence and presence of atrial-ventricular overlap. In Fig. 10a, the patient shows very little apparent overlapping of the left atrium and left ventricle, based on the cine display of the data. The first-harmonic phase pattern shows the septum to be relatively early, and the posterolateral wall to be later. This pattern is less common in normal wall-motion studies than that of Fig. 8. Figure 10b is from a different patient who has the same general phase pattern as the patient of Fig. 10a but who has a region at the base of the left ventricle where there is visible overlap of the left atrium. The phase image shows a pronounced change in phase in the region of the overlap. Also in this study, the first-harmonic phase functional image exhibits the free-wall phase shift illustrated by the phantom studies.

Different patterns appear in some of the multiharmonic functional images. In Fig. 4, the multiharmonic time of maximum shows a tighter span of values than the first harmonic. The absolute value of the time of maximum ranges much closer to the R wave, as is expected from its better fit to the data points. In Fig. 5, the time of maximum of the region of overlap is coded in a color intermediate between the two spheres. The multiharmonic time of onset of contraction, as determined by attainment of a significant fraction of the pixel stroke, is shown in Fig. 6. It is quite uniform in the "chambers." In the "septum" there are some subtle changes in value not evident in the first harmonic. Figure 7 displays the multiharmonic time of maximum for the translating sphere. A wide range of values appears, with a pattern that has smoother transitions in value than that of the first harmonic.

Multiharmonic functional images also show interesting patterns in patient data. In Fig. 9 the multiharmonic time of maximum is seen to have a broader range of values than the first harmonic and, in general, to be closer to the R wave. Figure 10c compares two multiharmonic images for the patient with overlap of the left atrium and left ventricle. The time-of-maximum image shows a marked change in color in the overlap region, just as the first-harmonic phase does. The image of the time of maximum negative rate of change shows very little influence from the overlap, coding most of the overlapped region in the same colors as the ventricle. Figure 11 is from a patient with septal akinesis and noticeable translation in the cine display. The time-of-maximum image shows a broad range of colors in the septal region. The maximum-excursion image shows that there is very little change in count rate in most of this area. The time-of-maximum image resembles the first-harmonic phase image (not illustrated), although, as with the translating phantom, the multiharmonic time of maximum shows a smoother transition on the patient's left side of the septum.

DISCUSSION

The first-harmonic approximation has been shown here and elsewhere to be a poor fit to the pixel time-activity curve. The phantom studies show how the inaccuracies of the fit affect the first-harmonic phase functional image. The same effects are observed in patient studies.

The cylindrical phantom in Fig. 3 gives a vivid example of the inadvisability of associating the time indi-

random phase, is coded black. LL is histogram of phase image. Phase histogram is quite typical, showing a peak corresponding to ventricles and located somewhat before R wave. Its precise location depends upon shape of pixel time-activity curves, and thus is related to heart rate. Atrial peak occurs about 180° from ventricular peak. Size of atrial peak is affected by magnitude value chosen for background masking, since great vessels tend to have phase values in same range. LR is end-diastolic frame for anatomical reference.

FIG. 9. (upper left, p 720) Patient demonstrating improved fit of multiharmonic approximation. He has relatively slow heart rate of 41 bpm. Count-rate profile below, color-coded by first-harmonic phase, shows resulting long diastolic period. First-harmonic phase functional image in UL has earlier colors than first-harmonic phase image of Fig. 8. Multiharmonic time-of-maximum image in UR has values much closer to R wave, suggesting that it may be more accurate as a measure of start of motion.

FIG. 10. (a) (upper right, p 720) Patient whose phase pattern is less frequently found among normals. Band of late phase along free wall of left ventricle is due to first-harmonic fit. Of special interest is absence of left atrial-ventricular overlap. UL is end-diastolic image and UR is end-systolic. LL is first-harmonic phase functional image and LR is its histogram. (b) (center left, p 720) Normal patient with phase pattern similar to (a). At base of left ventricle is region of atrial overlap. End-diastolic image is in UL and end-systolic in UR. First-harmonic phase image in LL shows region of overlap as a dark blue patch. (c) (center right, p 720) Same patient as (b) to compare multiharmonic time of maximum in UL with multiharmonic time of maximum negative slope in UR. Below, coded count-rate profile for multiharmonic time of maximum shows how atrial overlap causes a local peak in time-activity curves. In much of overlap region maximum negative slope image is unaffected by atrial contribution.

FIG. 11. (bottom left, p 720) Patient demonstrating pattern often found in septal akinesis. His scintigraphically determined ejection fraction is 0.29. Because change in counts due to ejection is so low, predominant change is result of translational motion, which can be seen in leftward shift of septum from end-diastole in UL to end-systole in UR. In maximum excursion image, superposition of ejection and translation is evident in small change in counts for much of septal side of left ventricle. Wisp of greater excursion near right ventricle is because edge of left ventricle moves into and out of pixels in septal region of end-diastolic frame. Effect on multiharmonic time-of-maximum functional image in LL is to produce large area of paradoxical values in septal region.

cated by the first-harmonic phase with the time at which contraction commences. The cylinder contracts radially, so the onset of contraction occurs earliest at its end-diastolic outline and latest at its end-systolic border. Just the opposite is observed in the first-harmonic phase image. The reason for this may be seen in the count-rate profile in Fig. 3. The pixel at the end-diastolic edge has the cylinder within its field of view for only a short part of the R-R interval. Consequently, the pixel's time-activity curve is quite symmetric about the R wave and the first-harmonic phase aligns itself with the R wave. For pixels closer to the center, the time-activity curve becomes less and less symmetric since the global volume curve is not symmetric. The effect on the first-harmonic phase is more clearly seen in Fig. 12. The point in the heart cycle marked A is the first-harmonic phase. As one moves toward the center of the phantom (from Fig. 12a to Fig. 12f), the phase (point A on the horizontal axis) shifts earlier. The Fourier approximation is a least-squares fit (*10*). Thus, the first harmonic tries to fit the valley and walls of the curve to minimize the sum of the squared deviations. As the valley narrows, the fit shifts in order to minimize the sum of the squared deviations as much as possible.

A similar effect appears in the spherical phantoms, although the center is slightly later in phase than the end-systolic border. This occurs because the pixel "stroke" is less within the end-systolic perimeter than at the end-systolic edge, so the first harmonic does not have to shift quite so far to fit the curve.

The rotating sphere with a "septum" in Fig. 6 exhibits a marked change in phase in the septum. This occurs because the edges of the chambers enter the septal region more toward end-systole, as is seen in the count-rate profile. Consequently, the time-activity curve for the septal pixels reaches a maximum when the rest of the sphere is at a minimum.

In Fig. 7 a similar effect occurs in the septal region of the translating phantom and at the free wall on the right side, the side toward which the sphere shifts. The translation effect upon the first-harmonic phase and multiharmonic time-of-maximum parameters is skewed. The side toward which the translation moves is later in value, and the side away from which the chamber moves is earlier.

The patient examples suggest that these same effects occur in clinical data and may account for many of the observed phase patterns.

As noted earlier, the patient in Fig. 8 shows an 80-msec spread in phase across the left ventricle. Clayton et al. (*8*) described the pattern of contraction of the normal human left ventricle on the basis of 30° RAO ventriculograms at 60 frames/sec. The observed pattern was a reduction in the transverse dimension of the ventricle before a shortening of the long axis, with the inferior wall moving before the anterior wall. In all but one

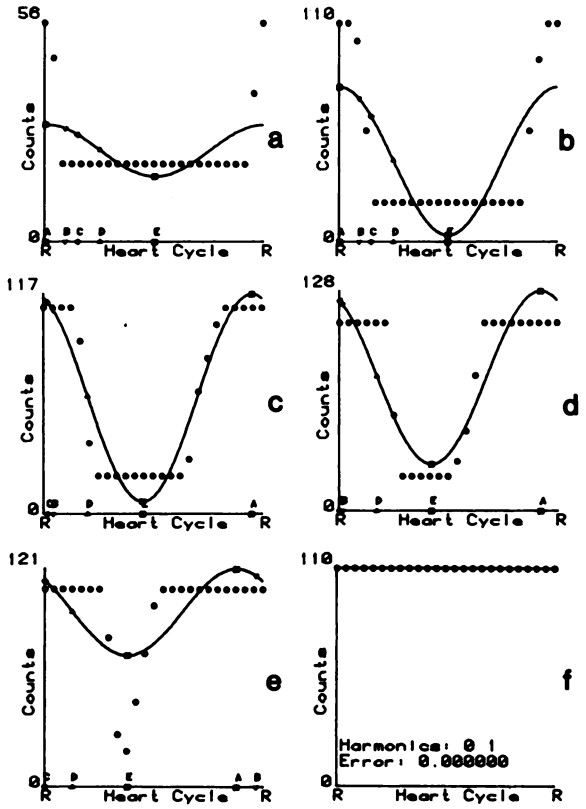

FIG. 12. (a) Pixel time-activity curve for pixel whose field of view encompasses edge of end-diastolic image of cylinder phantom. (b)–(d) Time-activity curves for pixels progressively closer to center of phantom volume. Effect on first-harmonic fit, which is most easily visualized by comparing point A in the different plots, makes it align with R wave in (a), but as time-activity curve becomes less and less symmetric, the fit shifts to left (i.e., earlier) in order to fit systolic trough.

patient, the apex was the last segment to contract. The duration of contraction of the left ventricle was typically about 25 msec. Another consistent explanation for the base-to-apex phase pattern observed in many normal patients is that the apex of the left ventricle is forced away from the base at the start of ventricular contraction and later the base follows the apex (*13*). Thus, one would see a rapid decrease in counts in the basal region and an initial increase in counts at the apex, as in the translating phantom. This has been observed in the study of Fig. 8. The effect on the phase image is that the base will have an earlier phase than the apex, owing to overall motion of the ventricle as well as to excitation and the greater symmetry near the edge of the chamber.

The patient in Fig. 9 has a long R-R interval. The pronounced shift of the first-harmonic phase before the R wave emphasizes that in absolute as well as in relative terms it is a poor indicator of the onset of contraction. The downward kick of the left-ventricular apex can be seen in the second trace of the count-rate profile as an increase in counts immediately after the R wave.

Figures 10a and 10b compare two patients with sim-

ilar phase patterns. In Fig. 10b there is significantly more overlap of the left atrium and left ventricle. This is reflected in the blue patch at the base of the left ventricle. Since the pixel time-activity curves are affected by both chambers, the phase of the first harmonic will fall somewhere in between, depending on the relative contributions of the two chambers to the time-activity curve.

Since the first-harmonic phase functional image has inherent edge effects, and moreover is sensitive to overall translation and rotation and to overlap of the chambers, it is appropriate to question its usefulness. There is considerable evidence that the first-harmonic phase is not without merit. In patients with bundle branch blocks, the ventricles have distinctly different phases. Patients with pacemakers are observed to have plausible patterns in the paced chambers (*6*,*11*). Encouraging results have been reported from the parametrization of the histograms of the first-harmonic phase distribution (*7*).

If all the pixel time-activity curves in a chamber were to have the same shape, and only the time at which contraction started were to differ, then the *relative* phases in the first-harmonic functional image would be exact. A problem occurs because the pixel time-activity curves, even for an instantaneously excited chamber like the spherical phantom, do not have the same shape everywhere in the chamber and thus produce markedly different first-harmonic phases. The different shapes arise because the image is a two-dimensional projection of a three-dimensional count distribution.

The problems with the first-harmonic approximation essentially are those of goodness of fit. By the orthogonality principle (*15*), the more terms that are included in the Fourier approximation, the better the fit will be (in a least-squares sense). Knowledge of the spectral content of typical time-activity curves dictates the best choice of terms in the multiharmonic approximation, Eq. (5).

The multiharmonic approximation has more than one pair of parameters (i.e., more than one magnitude and one phase), so it allows more than one unique temporal functional image. The Fourier approximation is an analytic function, so the type of multiharmonic calculation described above is readily performed. The multiharmonic parameters mentioned earlier are not an exhaustive list. With the ability to approximate the time-activity curve more accurately comes the ability to identify virtually any feature of the time-activity curve.

The phantoms and patient examples illustrate a few of the multiharmonic functional images, showing how they may or may not be desirable in a given situation. The multiharmonic time of maximum is the time at which the multiharmonic approximation has its maximum. In Fig. 4 it gives a more uniform functional image than the first-harmonic phase, because it is not nearly so sensitive to the symmetry of the time-activity curves. In the overlap region of Fig. 5, the time of maximum tracks the changes in the time-activity curve better than does the first-harmonic phase. In Fig. 7, whereas the pattern of the time of maximum has smoother transitions than that of the first-harmonic phase, it is still sensitive to the translation since the time-activity curves are changed so drastically. The time of maximum is applied to patient data in Figs. 9 and 11. Figure 9 shows the time of maximum to advantage and disadvantage. The left ventricle is much closer to the R wave, as one would want in a parameter indicative of the time of excitation. However, the distribution over the ventricle is not nearly so uniform as in the first-harmonic phase image. This patient has a long R-R interval, resulting in a long, flat later-diastolic period, as seen in the count-rate profile through the left ventricle. The result is that when the multiharmonic algorithm seeks the maximum, which occurs somewhere in the flat part of the time-activity curve, a very small change in counts produces a large change in the time of maximum. Thus, very little noise can produce a large uncertainty in the time of maximum. Figure 11 demonstrates that, just as in the phantom study, the time-of-maximum image is highly sensitive to translation.

The multiharmonic onset of contraction by excursion image in Fig. 6 shows the point in the R-R interval at which each pixel is unequivocally decreasing. Again, the chamber part of the phantom is more uniform than the first harmonic, since the onset image is sensitive only to the "systolic" part of the time-activity curves whereas the first-harmonic phase image is influenced by the entire time-activity curve. In the "septum" the multiharmonic onset parameter is more faithful to the shape of the time-activity curve. The count-rate profiles emphasize that the two edges of the septum have later "ejections" than the middle. The first-harmonic phase image does not reflect this.

Figure 10c compares images of the multiharmonic time of maximum and its negative rate of change. The latter is another multiharmonic parameter that relies on the systolic portion of the time-activity curve. In the region of left atrial-ventricular overlap, the time of maximum finds the point where the atrium is at a maximum. Since, in this case, the ventricular systolic part of the curve is relatively unaffected by the atrial contribution, most of the overlap region is identified as ventricle by the maximum negative slope parameter. In both cases, the absence of the free-wall "edge effect" can be noted in comparison with the first-harmonic phase in Fig. 10b.

A phase shift common to all approximations is inherent in the data-collection procedure. The first frame of the study is collected from the R wave until R-R interval/N, where N is the number of frames in the study. The Fourier transform, Eqs. (1) and (2), treats the first

point of the time-activity curve as if it occurred at time zero, whereas in fact it "occurred" at R-R interval/2N. Thus there is a systematic phase shift equal to one-half of one frame's duration. Since this is a constant shift for all studies with the same number of frames, and it affects the single and multiharmonic approximations equally, it has been ignored in the previous discussion.

The first-harmonic phase has two distinct advantages as a functional parameter. It is easy to compute, and hence cheap in terms of computer time (and does not even require the Fourier transform). Because it is extremely "low-pass" in the temporal dimension, it produces a smoother functional image. The multiharmonic approximation has a major advantage. It permits a wealth of unique functional parameters since it fits the pixel time-activity curve more accurately and has more than two independent parameters.

CONCLUSIONS

The first-harmonic phase functional image commonly used in the "phase analysis" of multigated cardiac blood-pool studies has been shown both in phantom data and in patient data to contain artifacts of the poor fit afforded by the first Fourier harmonic alone. Theory predicts that a better fit to the pixel time-activity curve is achieved by the use of additional harmonics in the approximation of the curve. Furthermore, because the multiharmonic approximation has more degrees of freedom, a variety of unique functional images is possible. A few multiharmonic functional images are compared with the first-harmonic phase images. In some situations, the more accurate approximation can be used advantageously. Because of the demonstrated inaccuracies of the first-harmonic approximation, caution is urged in the use of the first-harmonic phase image.

ACKNOWLEDGMENTS

We thank E. G. DePuey, R. E. Sonnemaker, S. E. Long, and W. L. Thompson for their helpful insight and C. Ridgell for his technical assistance.

APPENDIX: GENERATION OF THE PHANTOM STUDIES

The phantoms are generated from a global volume curve. In the case of the cylinder of constant thickness and varying radius, the radius of the image in frame k is

$$\text{radius}(k) = \sqrt{\frac{\text{volume}(k)}{\pi L}}, \quad (8)$$

where L is the length of the cylinder and k is the index indicating which frame of the phantom study is being computed.

For the spheres, the radius is

$$\text{radius}(k) = \left[\left(\frac{3}{4\pi}\right)\text{volume}(k)\right]^{-1/3}. \quad (9)$$

The value of a pixel is calculated by dividing the pixel into a 10 × 10 grid and computing the projected thickness at each point on the grid. For overlaps and rotations this involves the superposition of objects. The value of the thickness at each of the grid points is weighted by a "count density" and then the hundred values are summed to give the value of the pixel.

REFERENCES

1. ADAM WE, TARKOWSKA A, BITTER F, et al: Equilibrium (gated) radionuclide ventriculography. *Cardiovasc Radiol* 2:161-173, 1979
2. ALMASI JJ, BORNSTEIN I, EISNER RL, et al: Enhanced clinical utility of nuclear cardiology through advanced computer processing methods. *Computers in Cardiology Conference Proceedings* pp 397-400, 1979 (IEEE No. 79-CH1462-1C)
3. BACHARACH SL, GREEN MV, DE GRAAF CN, et al.: Fourier phase distribution maps in the left ventricle: Toward an understanding of what they mean. In *Functional Mapping of Organ Systems and Other Computer Topics* Esser PD, Ed. New York, Society of Nuclear Medicine, 1981, pp 139-148
4. BLACKMAN RB, TUKEY JW: *The Measurement of Power Spectra.* New York, Dover, 1958, pp 14-15
5. BOUGH EW, GANDSMAN EJ, SHULMAN RS: Measurement of normal left atrial function with gated radionuclide angiography. *Am J Cardiol* 48:473-478, 1981
6. BYROM E, SWIRYN S, PAVEL D, et al: Correlation of phase image patterns with various cardiac activation patterns induced by pacing. *J Nucl Med* 22:P18, 1981 (abst)
7. BYROM E, PAVEL DG, SWIRYN S, et al: Phase images of gated cardiac studies: A standard evaluation procedure. In *Functional Mapping of Organ Systems and Other Computer Topics.* Esser PD, Ed. New York, The Society of Nuclear Medicine, 1981, pp 129-138
8. CLAYTON PD, BULAWA WF, KLAUSNER SC, et al: The characteristic sequence for the onset of contraction in the normal human left ventricle. *Circulation* 59:671-679, 1979
9. CRAMER JA, EHRHARDT JC, COLLINS SM: Second harmonic analysis in the assessment of ventricular contraction patterns from radionuclide images. In *IEEE 1981 Frontiers of Engineering in Health Care.* Cohen BA, Ed. Houston, IEEE Engineering in Medicine and Biology Society, 1981, pp 97-101
10. DAVIS PJ: *Interpolation and Approximation.* Dover, New York, 1975, pp 158-200
11. FRAIS MA, BOTVINICK EH, O'CONNELL JW, et al: The phase image: An accurate means of detecting and localizing abnormal foci of ventricular activation. *J Nucl Med* 22:P18, 1981 (abst)
12. HAMMING RW: *Numerical Methods for Scientists and Engineers.* New York, McGraw-Hall, 1973, pp 68-72
13. MILNOR WR: The heart as a pump. In *Medical Physiology, Fourteenth Edition.* Mountcastle VB, Ed. St. Louis, Mosby, 1980, pp 986-1026
14. OPPENHEIM AV, SCHAFER RW: *Digital Signal Processing.* Englewood Cliffs, Prentice Hall, 1975
15. PAPOULIS A: *Probability, Random Variables, and Stochastic Processes.* New York, McGraw-Hill, 1965, pp 390-400
16. VERBA JW, BORNSTEIN I, ALAZRAKI NP, et al: Onset and progression of mechanical systole derived from gated radionuclide techniques and displayed in cine format. *J Nucl Med* 20:625-626, 1979 (abst)
17. WENDT RE, MURPHY PH, CLARK JW, et al: Fourier analysis of gated blood pool images. In *Proceedings of the 34th Annual Conference on Engineering in Medicine and Biology.* Houston, The Alliance for Engineering in Medicine and Biology, 1981, p 272